# Fault-Tolerant Tracking Control Optimization of Constrained LPV Systems Based on Embedded Preview Regulation and Reference Governance

Kezhen Han, Jian Feng, *Member, IEEE*, Yueyang Li, *Member, IEEE*, Ping Jiang, and Xiaohong Wang

***Abstract*—This article presents some new improvements to the relevant constrained predictive fault-tolerant tracking control (FTTC) methods through embedding optimal preview regulation and reference governance. The main novelty of such a strategy is that some valuable information of finite future references can be adequately scheduled to optimize the robust tracking performance and significantly enlarge the fault-tolerant admissible region. In order to better describe the wide applicability of the proposed strategy, the robust FTTC problem for a class of LPV systems with state/input constraints is considered. Overall, the involved key designs consist of three parts. First, an unconstrained FTTC component is constructed by combining tracking error feedback, reference input regulation, and fault signal compensation. It is used to guarantee the robust tracking stability of closed-loop systems when the constraints are not activated. Second, a tube-based predictive FTTC policy with an embedded optimal preview regulator is designed to achieve the robust constraint satisfaction and transient response improvement. Third, an embedded reference governor is additionally integrated to significantly enlarge the size of the fault-tolerant admissible region. This design further reinforces the feasibility of constrained FTTC optimization. The effectiveness of these results is finally validated by a case study of a single transistor dc/dc Forward converter.**

***Index Terms*—Constrained systems, constraint tightening, fault-tolerant tracking control (FTTC), preview control, reference governor (RG).**

## I. Introduction

IN THE pursuit of higher productivity, the complexity of today's industrial systems has increased dramatically. This generally brings more challenges to the design of control systems, as the probability of fault occurrence in complex systems increases significantly. In order to reduce the performance losses and avoid the system instability caused by faults, some effective measures should be taken. The fault-tolerant control (FTC) theory and method provide an effective way to improve the system reliability. Some representative results can be found in book [1], survey papers [2], [3], and the references therein. Particularly in recent years, the studies of FTC have been widely developed for various systems, such as T-S fuzzy system [4], formation flight system [5], uncertain system [6], switched system [7], etc.

FTC designs for systems with state/input constraints have been received much research interest in recent years [8], [9]. Compared to the problems encountered in typically unconstrained FTC studies, the constrained FTC scenarios are more difficult to handle since faults usually cause changes in the control input constraints and this may further modify the set of feasible solutions for a given control objective to be empty. Hence, apart from the basic robust stability requirement in unconstrained FTC, the real-time optimality and feasibility should be additionally fulfilled for constrained FTC. In order to acquire these multiperformances, the design method of constrained FTC must be constructed systematically.

Model predictive control (MPC) method provides an elegant solution to achieve the above constrained FTC since it has the inherent capacity to address the constrained optimization problem. Moreover, the implementation of MPC enables a nice property of smooth transition from faulty behavior to healthy behavior. This handling is beneficial to remove some serious transient influences of faults. On the contrary, there usually exists a large disturbance in response to fault accommodation if only a single signal compensation method is adopted to achieve the fault tolerance. The general advantages of MPC-based FTC methods have been discussed in [10] and [11] and many remarkable results have also been reported recently. For instance, a reliable fault-tolerant MPC strategy for drinking water transport networks was proposed in [12], where the discussions of structure, feasibility, performance, and reliability were given totally; the results of [12] were further developed by Zarch *et al.* [13] based on the viability theory; a predictive FTC strategy with fault detection units was designed to achieve the reliable longitudinal control of an Airbus passenger aircraft in [14]; the FTC problem of the LPV system with sensor faults was further addressed in [15]. The algorithm verifications in these FTC studies have demonstrated the powerful optimization capability of MPC-based fault accommodation within the constraints. However, these approaches are usually

Manuscript received 19 March 2022; accepted 13 April 2022. Date of publication 2 May 2022; date of current version 19 December 2022. This work was supported in part by the National Natural Science Foundation of China under Grant 61803178, Grant 61973135, and Grant 62173081; in part by the Shandong Provincial Natural Science Foundation under Grant ZR2019BF036; and in part by the Liaoning Revitalization Talents Program under Grant XLYC2002032. This article was recommended by Associate Editor Y. Song. *(Corresponding author: Kezhen Han.)*

Kezhen Han, Yueyang Li, Ping Jiang, and Xiaohong Wang are with the School of Electrical Engineering, University of Jinan, Jinan 250022, China (e-mail: hankezhen7758@163.com; cse_liyy@ujn.edu.cn; cse_jiangp@ujn.edu.cn; cse_wxh@ujn.edu.cn).

Jian Feng is with the College of Information Science and Engineering, Northeastern University, Shenyang 110819, China (e-mail: fjneu@163.com).

This article has supplementary material provided by the authors and color versions of one or more figures available at https://doi.org/10.1109/TSMC.2022.3168426.

Digital Object Identifier 10.1109/TSMC.2022.3168426

computationally demanding since most of them need to solve a multistep or complex numerical optimization at every control iteration. Therefore, it would be challenging when these methods are implemented to systems with fast dynamics or high sampling rates.

Fortunately, two popular ways have been formulated in the literature to relax the online computational requirements of MPC-based FTC. On the one hand, the multiparametric programming method is adopted to construct an explicit fault-tolerant MPC in [16] and [17]. In this strategy, the FTC laws for different fault situations should be calculated and stored in advance and only a recursive procedure for combining piecewise FTC laws is performed online. In general, this kind of FTC method can effectively speed up the fault accommodation. However, it may cause the storage difficulty, particularly for the situation where the available resources of the microcontroller, such as memory or register are limited. As an alternative scheme, the flexible dual-mode predictive paradigms have been received extensive attention recently in the field of FTC [18]. The essence of such dual-mode predictive FTC is to introduce a few online tunable variables on a fixed unconstrained FTC law. The unconstrained FTC law should be predesigned offline and used to guarantee the stability of the closed-loop system while the added tunable variables need to be determined online and used to handle constraints and perform optimization. In addition, the dual-mode approaches have straightforward guarantees of closed-loop stability whereas the conventional finite horizon approaches do not. The design procedure of dual-mode predictive FTC commonly relies on the construction of invariant set, in particular for ellipsoidal invariant set and polyhedral invariant set. For instance, a reference management-based dual-mode predictive FTC was proposed in [19], where a polyhedral invariant set was used to express the feasible region of constrained control problem. Recently, a standard dual-mode predictive FTC method was constructed based on the ellipsoidal invariant set and prediction augmentation in [18]. Later, the results of [18] were further developed by Witczak *et al.* [20] to optimize the regulation of a faulty wind turbine. In addition, the special concern of polyhedral invariant set-based dual-mode predictive FTC for LPV systems has also been given in [21], where a simultaneous state and fault estimation problem was also addressed. The simulation validations in these studies have demonstrated that the dual-mode predictive FTC methods can enjoy high computational efficiency and can provide reliable fault tolerance.

However, there are some unsatisfactory or even infeasible transient/steady-state responses of the above FTC methods when they are used to deal with the fault-tolerant problem of constrained tracking control for some changeable targets or references. The main reasons can be attributed to two aspects. On the one hand, their tracking control methods cannot capture the change trend of reference timely, which usually leads to the tracking delay of transient response. Moreover, the tracking accuracy would become much worse if the fault occurs at the same time as the change of reference. On the other hand, since the constrained feasibility of the above predictive FTC methods is regulated only by few online tunable variables, the fault-tolerant tracking objective could not be achieved once a slightly more serious fault or an abrupt/unreachable change of reference activates the constraint violation problem. In view of these observations, we attempt to find new solutions to improve the tracking accuracy as well as enhance the constrained feasibility of relevant fault-tolerant tracking control (FTTC) approaches. This is the main research motivation of this article.

The recent study [22] provides a promising insight to reinforce the typical dual-mode MPC of LTI systems by utilizing the information of reference or target in advance. Their conclusion has demonstrated that the suitable usage of future references can improve the tracking performance and feasibility of constrained optimization. Later, this method is further extended to deal with tracking control of an omnidirectional wheeled inverted pendulum in [23] and similar benefits are also captured. Inspired by their optimal reference scheduling applications, we attempt to extend this strategy to deal with the constrained FTTC optimization problem of LPV systems. However, the following major challenges are encountered during our expansion.

1) How to integrate the functions of FTTC and reference-based predictive regulation under the dual-mode prediction framework?
2) How to define and give the reasonable explanation about every component of the constrained dual-mode FTTC policy?
3) How to remove the negative influences of fault compensation errors and unknown disturbances on constrained optimization?
4) How to design the relevant feedback/feedforward gains and determine the optimal reference scheduling manner for LPV systems?

Taking the above problems into consideration, a novel robust constrained dual-mode predictive FTTC structure is proposed. A characteristic of this FTTC structure is the systematic integration of the advantages of the robust tracking control law, fault compensation policy, predictive perturbation, preview regulator (PR), and reference governor (RG). In principle, the robust tracking feedback control law is responsible for stabilizing the tracking error system whilst the fault compensation policy is responsible for eliminating the influence of faults directly. These two components constitute a robust unconstrained FTTC and their involved parameters should be designed offline under the framework of $H_\infty$ robustness optimization. In contrast, predictive perturbation, PR, and RG constitute the robust constrained FTTC and their values should be finally determined online. Overall, the predictive perturbation component is responsible to guarantee the basic constraint satisfaction of the lumped FTTC actions, and PR and RG are responsible to improve the corresponding transient- and steady-state tracking performance by making full use of finite previewable references. The systematical designs of the relevant parameters in constrained FTTC are achieved based on set theory method. In particular, the negative influences of fault compensation error and unknown disturbances on feasibility of overall FTTC are robustly suppressed through tightening the constraints. The above unconstrained FTTC part

and constrained FTTC part are unified under the framework of dual-mode predictive control and their cooperation can effectively address the aforementioned research motivations and objectives.

The main contribution of this research lies in the introduction and optimal utilization of PR and RG techniques to improve the transient tracking performance and fault-tolerant capacity of the existing constrained dual-mode predictive FTTC methods. Compared with the relevant studies [18]–[21], the main novelties and merits of proposed FTTC strategy can be summarized as follows.

1) The integration of PR allows the FTTC policy to take the suitable control action in advance such that the transient tracking response of closed-loop LPV system can be improved. This design becomes particularly prominent when the change of reference is accompanied by the appearance of fault.
2) The integration of embedded RG significantly enlarges the size of the fault-tolerant admissible region such that the robust feasibility of constrained FTTC optimization can be reinforced. This design would play a key role in ensuring the feasible fault tolerance when some large faults or fast changes of references lead to the unreachable tracking problem.

The validity of these conclusions is verified by a case study of a single transistor dc/dc forward converter.

The remainder of this article is structured as follows. Section II provides the problem formulation of constrained predictive FTTC. The corresponding analysis and synthesis are further given in Section III. Specifically, the strategies of unconstrained robust FTTC, PR-based robust predictive FTTC, and PR-RG-based robust predictive FTTC are explained and designed, respectively. In Section IV, several comparisons are given to validate the effectiveness of the proposed methods. Some conclusion and future work are discussed in Section V.

*Notations:* The symbol $\diamond$ represents the symmetric structure in a matrix. $X > 0$ (or $X < 0$) means that $X$ is square symmetric and $X$ is positive (or negative) definite. $X^{\mathrm{T}}$, $X^{-1}$ and $X^{+}$ denote the transpose matrix, inverse matrix, and generalized inverse matrix of $X$, respectively. $Co\{X_i\}, i = 1, 2, \ldots, h$ is the convex hull of $X_i$. $trace(X)$ is defined to be the sum of the main diagonal elements of $X$. $i \in \mathbb{N}_{[a,b]}$ denotes the nonnegative integers satisfying $a \le i \le b$. For two sets $p \in \mathbb{P}$ and $q \in \mathbb{Q}$, $\mathbb{P} \oplus \mathbb{Q} = \{p + q | p \in \mathbb{P},\ q \in \mathbb{Q}\}$ is the Minkowsi sum, and $\mathbb{P} \ominus \mathbb{Q} = \{p | p + q \in \mathbb{P} \quad \forall q \in \mathbb{Q}\}$ is the Pontryagin difference. Matrices, if their dimensions are not explicitly stated, are assumed to have compatible dimensions.

## II. Problem Formulation

Consider a class of tracking control problem of discrete-time LPV systems affected by unknown actuator faults and noises [15], [21], [24]

$$\begin{aligned} x_{k+1} &= A(\theta_k)x_k + B(\theta_k)(u_k + f_k) + D(\theta_k)\omega_k \\ y_k &= Cx_k,\ \text{s.t. } x_k \in \mathbb{X},\ u_k + f_k \in \mathbb{U} \end{aligned} \tag{1}$$

where $x_k \in \mathbb{R}^n$ represents the state vector and $y_k \in \mathbb{R}^m$ denotes the performance output. The actuator input is composed of $u_k$ and $f_k$, where $u_k \in \mathbb{R}^{n_u}$ is the control input vector and $f_k \in \mathbb{R}^{n_f}$ is the unknown actuator offset or drift fault vector. $\mathbb{X}$ and $\mathbb{U}$ are the constraint sets of states and actuator inputs. The system matrices $A(\theta_k)$, $B(\theta_k)$, and $D(\theta_k)$ are time-varying matrices that depend on scheduling parameter $\theta_k$. They are assumed to lie in a hypercube and can be represented by a convex combination of $h$ vertices, i.e., $\Gamma(\theta_k) = \sum_{i=1}^{h} \theta_{i,k}\Gamma_i,\ \Gamma_i \in \{A_i,\ B_i,\ D_i\}$, $\sum_{i=1}^{h} \theta_{i,k} = 1$.

*Remark 1:* In general, in terms of the design complexity of FTC methods and the effectiveness of their application, whether active or passive FTC is used depends on the degree of degradation of the influence caused by the fault on the performance of a given system. Taking actuator faults as an example, if the influence of certain actuator offset faults is slight, we can consider such faults as a disturbance and suppress them robustly by designing passive FTC methods. Conversely, if the offline simulation analysis indicates that the influence of actuator faults is large or cannot be ignored, active FTC methods should be used for targeted elimination and tolerance. The latter case is considered by default in this article.

Given the target or reference $y_{k+1} = r_{k+1}$, the operating point (i.e., the relevant state $x_{r,k}$ and control input $u_{r,k}$) can be determined by $\begin{bmatrix} x_{r,k} \\ u_{r,k} \end{bmatrix} = \begin{bmatrix} A(\theta_k) - I & B(\theta_k) \\ C & 0 \end{bmatrix}^{+} \begin{bmatrix} 0 \\ r_{k+1} \end{bmatrix}$, which defines $x_{r,k} = K_{xr}(\theta_k)r_{k+1}$ and $u_{r,k} = K_{ur}(\theta_k)r_{k+1}$.

*Assumption 1:* The LPV system (1) is stabilizable; the state vector $x_k$ is available to the controller; and $\theta_k$ is available online and not affected by faults.

*Assumption 2:* The reference $r_k$ is previewable with finite preview horizon $n_r$; the current and finite future values of reference $(r_k, r_{k+1}, \ldots, r_{k+n_r})$ are available at every moment.

*Assumption 3:* The disturbance vector $\omega_k$ is known to lie in a compact and convex set $\mathbb{W} = \{\omega | |\omega_k| \le \varrho_\omega\}$; the vector of fault change rate $\delta_{f,k} = f_{k+1} - f_k$ is also assumed to lie in a compact and convex set $\mathbb{F} = \{\delta_f | |\delta_{f,k}| \le \varrho_f\}$.

*Remark 2:* Assumption 1 is common in the fault diagnosis and FTC studies of LPV systems [21], [25]–[27]. For simplification, the states are deemed to be accessible directly. Otherwise, observer methods can be utilized to provide state estimation [28]–[33]. Assumption 2 implies that we have the potential to improve the FTTC performance by taking advantage of advance information of references [34].

*Remark 3:* Some additional clarification of Assumption 3 is required. First, Assumption 3 is mainly used to quantify the maximum negative impact of disturbances and faults on control performance and it is commonly given in robust MPC-based FTC studies (e.g., [18]–[21]). In many scenarios, the upper bounds of disturbances and the fault change rates can be determined through model analysis or identification technique. At least, according to the operational requirements and characteristics of the plant, certain suitable values can be selected in advance to assume the range of disturbances or severity of faults that can be tolerated. However, if it is difficult to determine such upper bounds in some practical systems, the original constraints sets will no longer be tightened in the subsequent design of predictive FTC. In this case, the

robustness and feasibility of FTC under constraints will be reduced significantly.

The objective is to design an optimal constrained predictive FTTC policy such that the output $y_k$ can be steered to track $r_k$ in a way of minimizing the cost function (2) at all times

$$\mathcal{J}_k = \sum_{t=0}^{\infty} U(x_{k+t}, u_{k+t}),\ \text{s.t.}\ x_{k+t} \in \mathbb{X},\ u_{k+t} + f_{k+t} \in \mathbb{U} \quad (2)$$

where $U(x_{k+t}, u_{k+t}) = (x_{k+t} - x_{r,k+t})^{\mathrm{T}} Q (x_{k+t} - x_{r,k+t}) + (u_{k+t} + f_{k+t} - u_{r,k+t})^{\mathrm{T}} R (u_{k+t} + f_{k+t} - u_{r,k+t})$ is a utility function with weighting matrices $Q > 0$ and $R > 0$.

To optimize (2) with sufficient feasibility and high computational efficiency, a novel constrained robust predictive FTTC policy is constructed via integrating optimal PR and RG in predictive input $c_k$

$$\begin{aligned} u_k &= K_e(x_k - x_{r,k}) + u_{r,k} - \hat{f}_k + c_k \\ c_k &= K_c \vec{\eta}_k + K_r \vec{r}_{k+1} \end{aligned} \quad (3)$$

where $K_e(x_k - x_{r,k}) + u_{r,k}$ is a robust tracking control law used to achieve the closed-loop stability of the tracking error system; $\hat{f}_k$ is a fault estimate and it is directly used to achieve fault signal compensation by $-\hat{f}_k$; and $c_k$ is the optimal predictive input that is used to handle constraints and ensure the feasibility of optimization problem (2). Note that the prediction of FTTC (3) follows the dual-mode mechanism as:

$$u_{k+i} - u_{r,k+i} = \begin{cases} K_e(x_{k+i} - x_{r,k+i}) - \hat{f}_{k+i} + K_c \vec{\eta}_{k+i} + K_r \vec{r}_{k+i+1} & \forall i \in \mathbb{N}_{[0,n_c-1]} \\ K_e(x_{k+i} - x_{r,k+i}) - \hat{f}_{k+i} + \zeta_{k+i} + K_r \vec{r}_{k+i+1} & \forall i \geq n_c \end{cases} \quad (4)$$

where $K_r \vec{r}_{k+1}$ is the optimal PR that is formulated to improve the transient-state behavior. $\zeta_k$ enables the embedded RG and it is used to reinforce the steady-state feasibility of constrained optimization. The predictive perturbation $K_c \vec{\eta}_k = \begin{bmatrix} I & 0 \end{bmatrix} \vec{\eta}_k = \eta_k$ puts the first optimal move of $\vec{\eta}_k$ into $u_k$ and it is used to guarantee the constraint satisfaction of transient-state response. Note that the feedback gain $K_e$ and feedforward gain $K_r$ would be designed offline. On the contrary, the variables $\eta_k$ and $\zeta_k$ should be searched online. The augmented vectors involved in (4) are defined as $\vec{c}_k = \begin{bmatrix} c_k^{\mathrm{T}} & c_{k+1}^{\mathrm{T}} & \cdots & c_{k+n_c-1}^{\mathrm{T}} \end{bmatrix}^{\mathrm{T}}$, $\vec{\eta}_k = \begin{bmatrix} \eta_k^{\mathrm{T}} & \eta_{k+1}^{\mathrm{T}} & \cdots & \eta_{k+n_c-1}^{\mathrm{T}} \end{bmatrix}^{\mathrm{T}}$, and $\vec{r}_{k+1} = \begin{bmatrix} r_{k+1}^{\mathrm{T}} & r_{k+2}^{\mathrm{T}} & \cdots & r_{k+n_r}^{\mathrm{T}} \end{bmatrix}^{\mathrm{T}}$, respectively.

*Remark 4:* Although both $\eta_k$ and $\zeta_k$ are used to guarantee the robust constrained feasibility of system behavior, they have different regulation mechanisms. This can be explained based on the observation of the prediction window in (4), as $\eta_k$ works in the transient mode $\forall i \in \mathbb{N}_{[0,n_c-1]}$ while $\zeta_k$ mainly impacts the terminal mode $\forall i \geq n_c$.

## III. Main Results

In this section, we will explain how to systematically integrate PR and RG into predictive FTTC (3) and (4) and how to determine the optimal parameters involved. In order to better describe the function of each component, three FTTC strategies are extracted from FTTC (3) and (4), namely, unconstrained robust FTTC, PR-based robust predictive FTTC, and PR- and RG-based robust predictive FTTC. In the sequel, the specific analysis and design conditions are given gradually.

### A. Design of Unconstrained Robust FTTC

According to (3), an unconstrained robust FTTC strategy is constructed as $u_k^{un} = K_e(x_k - x_{r,k}) + u_{r,k} - \hat{f}_k$. First, the fault estimation is given to enable fault compensation. It is observed from (1) that $d_k = x_{k+1} - A(\theta_k)x_k - B(\theta_k)u_k = B(\theta_k)f_k + D(\theta_k)\omega_k$. We then have $B(\theta_k)f_k = d_k - D(\theta_k)\omega_k$ that implies $f_k = H(\theta_k)(d_k - D(\theta_k)\omega_k)$ with $H(\theta_k) = (B^{\mathrm{T}}(\theta_k)B(\theta_k))^{-1}B^{\mathrm{T}}(\theta_k)$. As $\omega_k$ is unknown and $d_k$ relies on one-step ahead measurement $x_{k+1}$, $f_k$ cannot be directly estimated by $H(\theta_k)(d_k - D(\theta_k)\omega_k)$. A practical method is to use its approximate estimation [18]

$$\hat{f}_k = H(\theta_{k-1})d_{k-1}. \quad (5)$$

This treatment would bring certain fault compensation error. Fortunately, we can determine its bound according to Assumption 3. Clearly, there is $e_{f,k} = f_k - \hat{f}_k = f_k - (f_{k-1} + H(\theta_{k-1})D(\theta_{k-1})\omega_{k-1}) = \delta_{f,k} - H(\theta_{k-1})D(\theta_{k-1})\omega_{k-1} \in \mathbb{F} \oplus (-H(\theta_{k-1})D(\theta_{k-1}))\mathbb{W}$. To present a suitable set description of $e_{f,k}$, the term $H(\theta_{k-1})D(\theta_{k-1})$ can be simplified by

$$\begin{aligned} H(\theta_{k-1})D(\theta_{k-1}) &= \left(\sum_{i=1}^{h} \theta_{i,k-1} H_i\right)\left(\sum_{i=1}^{h} \theta_{i,k-1} D_i\right) \\ &= \underbrace{\begin{bmatrix} H_1 & H_2 & \cdots & H_h \end{bmatrix}}_{\mathcal{H}} \begin{bmatrix} \theta_{1,k-1} I \\ \theta_{2,k-1} I \\ \vdots \\ \theta_{h,k-1} I \end{bmatrix} \begin{bmatrix} \theta_{1,k-1} I \\ \theta_{2,k-1} I \\ \vdots \\ \theta_{h,k-1} I \end{bmatrix}^{\mathrm{T}} \underbrace{\begin{bmatrix} D_1 \\ D_2 \\ \vdots \\ D_h \end{bmatrix}}_{\mathcal{D}}. \end{aligned} \quad (6)$$

Due to $\theta_{i,k-1} \in [0,\ 1]$, there is $\|H(\theta_{k-1})D(\theta_{k-1})\| \leq \|\mathcal{H}\mathbf{1}_{nh}\mathcal{D}\|$, where $\mathbf{1}_{nh}$ denotes a $nh$-by-$nh$ matrix full of ones. Then, we can further redefine the set constraint of fault estimation/compensation error by $e_{f,k} \in \mathbb{F} \oplus (-\mathcal{H}\mathbf{1}_{nh}\mathcal{D}\mathbb{W})$.

In the sequel, the error feedback gain $K_e$ is designed in an optimization way such that the robust stability of tracking error system is guaranteed and the cost function (2) is minimized simultaneously. For such a purpose, an artificial output equation is constructed based on the utility function of (2)

$$z_k = C_z e_{x,k} + B_z e_{u,k},\ C_z = \begin{bmatrix} Q^{1/2} \\ 0 \end{bmatrix},\ B_z = \begin{bmatrix} 0 \\ R^{1/2} \end{bmatrix} \quad (7)$$

where $e_{x,k} = x_k - x_{r,k}$ and $e_{u,k} = u_k + f_k - u_{r,k}$. Clearly, there is $U(x_k, u_k) = z_k^{\mathrm{T}} z_k$. Next, by feeding (1) and (7) with unconstrained FTTC input $u_k^{un}$, we can obtain the closed-loop tracking error dynamics

$$e_{x,k+1} = \Phi(\theta_k)e_{x,k} + \bar{B}(\theta_k)v_k,\ z_k = \bar{C}e_{x,k} + \bar{D}v_k \quad (8)$$

where $\Phi(\theta_k) = A(\theta_k) + B(\theta_k)K_e$, $\bar{B}(\theta_k) = \begin{bmatrix} B(\theta_k) & D(\theta_k) \end{bmatrix}$, $\bar{C} = C_z + B_z K_e$, $\bar{D} = \begin{bmatrix} B_z & 0 \end{bmatrix}$, and $v_k = \begin{bmatrix} e_{f,k}^{\mathrm{T}} & \omega_k^{\mathrm{T}} \end{bmatrix}^{\mathrm{T}}$.

Based on the above analysis, the design conditions of feedback gain $K_e$ are summarized in Theorem 1.

*Theorem 1:* Given the LPV system (1) without constraints and the cost function (2), there exists a robust unconstrained FTTC policy $u_k^{un}$ such that the closed-loop LPV system is

stabilized and the cost function is minimized in the manner of $H_\infty$ performance optimization, if the matrix variables $P_i = P_i^{\mathrm{T}} > 0$, $G$, and $\bar{K}_e$ exist as solutions to the following minimization problem:

$$\gamma^* := \min\ \gamma \quad \text{s.t.} \begin{bmatrix} P_i - G - G^{\mathrm{T}} & \diamond & \diamond & \diamond \\ 0 & -\gamma^2 I & \diamond & \diamond \\ A_i G + B_i \bar{K}_e & \bar{B}_i & -P_j & \diamond \\ C_z G + B_z \bar{K}_e & \bar{D} & 0 & -I \end{bmatrix} < 0 \quad \forall i, j = 1, 2, \ldots, h. \tag{9}$$

Once (9) is solved, an optimized tracking error feedback gain can be determined by $K_e = \bar{K}_e G^{-1}$.

*Proof:* Let $V_{x,k} = e_{x,k}^{\mathrm{T}} P^{-1}(\theta_k) e_{x,k}$ be a candidate of the Lyapunov function of (8). Then, using the relaxation $-G^{\mathrm{T}} P_i^{-1} G \le P_i - G - G^{\mathrm{T}}$ and performing congruence transformation with $\mathrm{diag}\{(G^{\mathrm{T}})^{-1}, I, I, I\}$ and its transpose, the inequality in (9) guarantees $\begin{bmatrix} -P_i^{-1} & \diamond & \diamond & \diamond \\ 0 & -\gamma^2 I & \diamond & \diamond \\ A_i + B_i K_e & \bar{B}_i & -P_j & \diamond \\ C_z + B_z K_e & \bar{D} & 0 & -I \end{bmatrix} < 0$. Furthermore, based on the Schur complement lemma, there is $\begin{bmatrix} -P_i^{-1} & \diamond \\ 0 & -\gamma^2 I \end{bmatrix} - \begin{bmatrix} A_i + B_i K_e & \bar{B}_i \\ C_z + B_z K_e & \bar{D} \end{bmatrix}^{\mathrm{T}} \begin{bmatrix} -P_j & \diamond \\ 0 & -I \end{bmatrix}^{-1} \begin{bmatrix} A_i + B_i K_e & \bar{B}_i \\ C_z + B_z K_e & \bar{D} \end{bmatrix} < 0$. Given $\begin{bmatrix} e_{x,k}^{\mathrm{T}} & v_k^{\mathrm{T}} \end{bmatrix}^{\mathrm{T}}$, the above inequality further guarantees

$$\begin{bmatrix} e_{x,k} \\ v_k \end{bmatrix}^{\mathrm{T}} \left\{ \begin{bmatrix} -P^{-1}(\theta_k) & \diamond \\ 0 & -\gamma^2 I \end{bmatrix} + \begin{bmatrix} A(\theta_k) + B(\theta_k) K_e & \bar{B}(\theta_k) \\ C_z + B_z K_e & \bar{D} \end{bmatrix}^{\mathrm{T}} \begin{bmatrix} P^{-1}(\theta_{k+1}) & \diamond \\ 0 & I \end{bmatrix} \begin{bmatrix} A(\theta_k) + B(\theta_k) K_e & \bar{B}(\theta_k) \\ C_z + B_z K_e & \bar{D} \end{bmatrix} \right\} \begin{bmatrix} e_{x,k} \\ v_k \end{bmatrix} < 0.$$

Clearly, when $v_k = 0$, there is $V_{x,k+1} - V_{x,k} < 0$, which validates the stability of nominal closed-loop LPV system. When $v_k \neq 0$, it is straightforward to deduce $V_{x,k+1} - V_{x,k} + z_k^{\mathrm{T}} z_k - \gamma^2 v_k^{\mathrm{T}} v_k < 0$. Furthermore, by summing up both sides of this inequality from $k = 0$ to $k = +\infty$, there is $\|z_k\|_2^2 \le \gamma^2 \|v_k\|_2^2$ under the assumption of zero-initial conditions, which suggests that the robust stability of closed-loop LPV systems in the sense of $H_\infty$ performance requirement can be satisfied. In addition, according to the relation $U(x_k, u_k) = z_k^{\mathrm{T}} z_k$, we also have $\mathcal{J}_{x_k,u_k} \le \gamma^2 \|v_k\|_2^2$. Clearly, the tracking performance evaluation of cost function (2) obtained by using $u_k^{un}$ can be optimized if $K_e$ is designed under the condition of minimizing $\gamma$. The proof of Theorem 1 is completed. ∎

*Remark 5:* The optimization problem in Theorem 1 is a semidefinite programming (SDP) problem, and whether this SDP problem has a solution depends on whether LMI constraint in (9) is feasible. Since LMI in (9) is derived following the analytical method of the bounded real lemma, the existence of a solution to its corresponding algebraic Riccati or Lyapunov equation is a necessary condition for its feasibility. Further considering that the relaxation lemma is used in the derivation, a sufficient condition for the existence of a solution to this optimization problem is the existence of $(P_i = P_i^{\mathrm{T}} > 0, K_e)$ such that the system (8) is stabilizable and the existence of a nonsingular $G$ such that $P_i - G - G^{\mathrm{T}} < 0$.

### B. Design of PR-Based Robust Predictive FTTC

The determination of PR gain $K_r$ depends on the component analysis of variable $c_k$ in (3). As explained earlier, $c_k$ is used to ensure the feasibility of constrained FTTC. Here, we assume that the parameterization of $c_k = K_c \vec{\eta}_k + K_r \vec{r}_{k+1}$ in (3) is previously unknown. In order to characterize this situation, a new predictive FTTC policy $u_k^c = K_e(x_k - x_{r,k}) + u_{r,k} + c_k - \hat{f}_k$ is defined. In the sequel, $u_k^c$ is used to control the LPV systems. Without loss of generality, a hypothetical steady state $x_{r,k} = x_{r,k+1}$ can be set for given reference. In this case, the relevant tracking error dynamics can be modeled as $x_{k+1} - x_{r,k} = A(\theta_k)(x_k - x_{r,k}) + B(\theta_k)(u_k^c + f_k - u_{r,k}) + D(\theta_k)\omega_k \Rightarrow x_{k+1} = \Phi(\theta_k) x_k + (I - \Phi(\theta_k)) K_{xr}(\theta_k) r_{k+1} + B(\theta_k) c_k + \bar{B}(\theta_k) v_k$. By considering $c_k = K_c \vec{c}_k$ and $r_{k+1} = C_r \vec{r}_{k+1}$, the above equation can be further rewritten as

$$\begin{aligned} x_{k+1} = {} & \Phi(\theta_k) x_k + (I - \Phi(\theta_k)) K_{xr}(\theta_k) C_r \vec{r}_{k+1} \\ & + B(\theta_k) K_c \vec{c}_k + \bar{B}(\theta_k) v_k \end{aligned} \tag{10}$$

where $K_c = \begin{bmatrix} I_{n_u \times n_u} & 0 \end{bmatrix}$ and $C_r = \begin{bmatrix} I_{m \times m} & 0 \end{bmatrix}$.

The following invariant set definitions are referred from [35] and used to facilitate the subsequent discussions about closed-loop stability and feasibility of (10).

*Definition 1:* A set $\mathbb{S}_{RPI} \subseteq \mathbb{X}$ is a robust positive invariant set (RPI-set) for an autonomous model of system (10) (i.e., $K_c \vec{c}_k = 0$) subject to constraint $x_k \in \mathbb{X}$, if for any $x_0 \in \mathbb{S}_{RPI}$, we have $x_k \in \mathbb{S}_{RPI}$ for all $\bar{B}(\theta_k) v_k \in \Delta$, $k \ge 0$. Moreover, $\mathbb{S}_{MRPI}$ is the maximal RPI-set if $\mathbb{S}_{MRPI}$ contains all the RPI-sets of constrained autonomous system (10) in $\mathbb{X}$.

*Definition 2:* A set $\mathbb{S}_{RCI} \subseteq \mathbb{X}$ is a robust control invariant set (RCI-set) for nonautonomous system (10) (i.e., $K_c \vec{c}_k \neq 0$) subject to constraints ($x_k \in \mathbb{X}$, $u_k \in \mathbb{U}$) if for any $x_0 \in \mathbb{S}_{RCI}$, there exists control input $u_k \in \mathbb{U}$ such that all the state updates satisfy $x_k \in \mathbb{S}_{RCI}$ for all $\bar{B}(\theta_k) v_k \in \Delta$, $k \ge 0$. Similarly, the maximal RCI-set $\mathbb{S}_{MRCI}$ contains all robust RCI-sets.

According to Assumption 2, a dynamic model of previewable reference vector can be established as $\vec{r}_{k+2} = A_r \vec{r}_{k+1}$, where $A_r = \begin{bmatrix} 0 & I \\ 0 & I \end{bmatrix}$. Note that when constructing $A_r$, we have assumed that the change of reference beyond $r_{k+n_r}$ has little effect on current decision and $r_{k+n_r}$ reaches the terminal desired set point (i.e., $r_{k+n_r+1} = r_{k+n_r}$). In addition, according to the operating mechanism of dual-mode predictive control scheme, we also assume that the prediction of states beyond $k + n_c$ has entered into the terminal $\mathbb{S}_{RPI}$ and in this case $c_{k+n_c}$ becomes 0. With this in mind, we can further construct a dynamic model of $\vec{c}_k$ as $\vec{c}_{k+1} = A_c \vec{c}_k$, where $A_c = \begin{bmatrix} 0 & I \\ 0 & 0 \end{bmatrix}$.

Next, by defining $Z_k = \begin{bmatrix} x_k^{\mathrm{T}} & \vec{c}_k^{\mathrm{T}} & \vec{r}_{k+1}^{\mathrm{T}} \end{bmatrix}^{\mathrm{T}}$, the following augmented model can be obtained:

$$Z_{k+1} = \Psi(\theta_k) Z_k + \tilde{B}(\theta_k) v_k \tag{11}$$

where $\Psi(\theta_k) = \begin{bmatrix} \Phi(\theta_k) & B(\theta_k) K_c & (I - \Phi(\theta_k)) K_{xr}(\theta_k) C_r \\ 0 & A_c & 0 \\ 0 & 0 & A_r \end{bmatrix}$ and $\tilde{B}(\theta_k) = \begin{bmatrix} \bar{B}^{\mathrm{T}}(\theta_k) & 0 & 0 \end{bmatrix}^{\mathrm{T}}$.

The above augmentation enables that the determination of $\mathbb{S}_{MRCI}$ of (10) can be achieved by calculating the projection of $\mathbb{S}_{MRPI}$ of (11) on $x_k$. Before that, the tube-based method is adopted to tighten the constraints ($\mathbb{X}$, $\mathbb{U}$) such that the influences of fault compensation error and disturbance on the feasibility of FTTC can be excluded. First, in (8) and (10), it shows $\bar{B}(\theta_k)v_k = B(\theta_k)e_{f,k} + D(\theta_k)\omega_k$. According to Assumption 3 and the fault estimation in (5), there is $\bar{B}(\theta_k)v_k \in \Delta = Co\{B_i\mathbb{F}\} \oplus Co\{-B_i\mathcal{H}\mathbf{1}_{nh}\mathcal{D}\mathbb{W}\} \oplus Co\{D_i\mathbb{W}\}$, $i = 1, 2, \ldots, h$. By using $\Delta$ to stimulate (10) in a set iteration way, an approximate disturbance invariant set $\mathbb{X}_\delta$ can be determined to describe the bound of response to fault compensation error and disturbance. Note that in the above calculations, we should set $\vec{r}_{k+1} = 0$ and $\vec{c}_k = 0$. Then, an intuitive manner to remove the negative impact of $\Delta$ is to tighten the constraints by $\bar{\mathbb{X}} = \mathbb{X} \ominus \mathbb{X}_\delta$ and $\bar{\mathbb{U}} = \mathbb{U} \ominus K_e\mathbb{X}_\delta$. This handling enables that the predictive FTTC problem of (11) is further robustly transformed into the predictive FTTC problem of the following:

$$Z_{k+1} = \Psi(\theta_k)Z_k, \text{ s.t. } K_{zx}Z_k \in \bar{\mathbb{X}}, \ K_{zu}Z_k \in \bar{\mathbb{U}} \tag{12}$$

where $K_{zx} = \begin{bmatrix} I & 0 & 0 \end{bmatrix}$ and $K_{zu} = \begin{bmatrix} K_e & K_c & (K_{ur}(\theta_k) - K_eK_{xr}(\theta_k))C_r \end{bmatrix}$.

*Remark 6:* Based on the problem transformations from (10) to (12), the influences of fault compensation error and disturbance have been characterized by disturbance invariant set $\mathbb{X}_\delta$. The admissible feasible region of $x_k$ that excludes $\mathbb{X}_\delta$ has also been contained in $\mathbb{S}_{MRPI}$ of (12). The fault-tolerant ability of $u_k^c$ can thus be reflected via evaluating the projection volume of $\mathbb{S}_{MRPI}$ of (12) on its first component $x_k$. In other words, we can use such a projection set to represent the fault-tolerant admissible region. For the sake of simplicity, the fault-tolerant admissible region is denoted as $\mathbb{S}_{\text{FTAR}}$. Clearly, for given set point or reference, the degrees of freedom provided by $\vec{c}_k$ decide the volume of $\mathbb{S}_{\text{FTAR}}$.

According to Definitions 1 and 2 and Remark 6, the set $\mathbb{S}_{\text{FTAR}}$ of (12) can thus be established as

$$\mathbb{S}_{\text{FTAR}}^c = \left\{x : \exists \vec{c}_k, \text{ s.t. } \mathcal{M}^c x_k + \mathcal{N}^c\vec{c}_k + \mathcal{P}^c\vec{r}_{k+1} \le b^c\right\} \tag{13}$$

where the involved parameters $\mathcal{M}^c$, $\mathcal{N}^c$, $\mathcal{P}^c$, and $b^c$ can be calculated by using the algorithm in [36].

Based on $u_k^c$ and (12), the minimization of cost function (2) (i.e., $\min_u \mathcal{J}_k$) can be rewritten as

$$\begin{aligned} \min_{\vec{c}_k} & \sum_{i=0}^{\infty} Z_{k+i}^{\mathrm{T}}\left[\Gamma_x^{\mathrm{T}}(\theta_k)Q\Gamma_x(\theta_k) + \Gamma_u^{\mathrm{T}}(\theta_k)R\Gamma_u(\theta_k)\right]Z_{k+i} \\ & \Gamma_x(\theta_k) = \begin{bmatrix} I & 0 & -K_{xr}(\theta_k)C_r \end{bmatrix} \\ & \Gamma_u(\theta_k) = \begin{bmatrix} K_e & K_c & -K_eK_{xr}(\theta_k)C_r \end{bmatrix}. \end{aligned} \tag{14}$$

According to the Lyapunov stability principle, the upper limit of cost function (14) for given $Z_k$ can be bounded by a suitable quadratic term $\bar{\mathcal{J}}_k = Z_k^{\mathrm{T}}SZ_k$. Without loss of generality, the symmetric matrix $S$ can be rewritten in the form of block-structured submatrices $\begin{bmatrix} S_{11} & S_{12} & S_{13} \\ \diamond & S_{22} & S_{23} \\ \diamond & \diamond & S_{33} \end{bmatrix}$. Based on such a division, $\bar{\mathcal{J}}_k$ can be further expanded as

$$\begin{aligned} \bar{\mathcal{J}}_k = {} & x_k^{\mathrm{T}}S_{11}x_k + 2x_k^{\mathrm{T}}S_{12}\vec{c}_k + 2x_k^{\mathrm{T}}S_{13}\vec{r}_{k+1} + \vec{c}_k^{\mathrm{T}}S_{22}\vec{c}_k \\ & + 2\vec{c}_k^{\mathrm{T}}S_{23}\vec{r}_{k+1} + \vec{r}_{k+1}^{\mathrm{T}}S_{33}\vec{r}_{k+1} \end{aligned} \tag{15}$$

where the links among $x_k$, $\vec{c}_k$, and $\vec{r}_{k+1}$ are shown. Clearly, we can ignore the terms $x_k^{\mathrm{T}}S_{11}x_k$, $2x_k^{\mathrm{T}}S_{13}\vec{r}_{k+1}$, and $\vec{r}_{k+1}^{\mathrm{T}}S_{33}\vec{r}_{k+1}$ since they contain no DOF relevant to the optimization of $\bar{\mathcal{J}}_k$. Then, $\min_{\vec{c}_k} \bar{\mathcal{J}}_k$ is equivalent to $\min_{\vec{c}_k} \tilde{J}_k = \{2x_k^{\mathrm{T}}S_{12}\vec{c}_k + \vec{c}_k^{\mathrm{T}}S_{22}\vec{c}_k + 2\vec{c}_k^{\mathrm{T}}S_{23}\vec{r}_{k+1}\}$. An immediate way to obtain the optimal value of $\vec{c}_k$ is to solve its derivative equilibrium equation

$$\frac{\mathrm{d}\tilde{J}_k}{\mathrm{d}\vec{c}_k} = 0 \Rightarrow \vec{c}_k = -S_{22}^{-1}\left(S_{23}\vec{r}_{k+1} + S_{12}^{\mathrm{T}}x_k\right). \tag{16}$$

In order to maintain the characteristic of the dual-mode predictive paradigm, we should restrict that $\vec{c}_k$ is not explicitly relevant to states and must provide a perturbation term simultaneously. Thus, the following parameterization of (16) is defined:

$$\vec{c}_k = \vec{\eta}_k + K_p\vec{r}_{k+1}, \ K_p = -S_{22}^{-1}S_{23}, \ S_{12} = 0 \tag{17}$$

where $\vec{\eta}_k$ is a new perturbation embedded in $\vec{c}_k$. In addition, the summation of each row elements of $K_p$ should be equal to 0. This follows immediately from the observation that if the reference is unchangeable then the optimum unconstrained predictive input value should satisfy $\vec{c}_k = 0$. In this case, we need to set $\vec{\eta}_k = 0$ and $K_p\vec{r}_{k+1} = 0$.

Now, based on (17), a simplified optimization of the cost function can be finally established in Lemma 1.

*Lemma 1:* The minimization of cost function (2) gives the same optimum $\vec{c}_k$ of the following optimization:

$$\min_{\vec{\eta}_k} \breve{\mathcal{J}}_k = \vec{\eta}_k^{\mathrm{T}}S_{22}\vec{\eta}_k, \ \vec{c}_k = \vec{\eta}_k + K_p\vec{r}_{k+1}. \tag{18}$$

*Proof:* By substituting (17) into $\tilde{J}_k$, there is $\vec{c}_k^{\mathrm{T}}S_{22}\vec{c}_k + 2\vec{c}_k^{\mathrm{T}}S_{23}\vec{r}_{k+1} = \vec{\eta}_k^{\mathrm{T}}S_{22}\vec{\eta}_k + 2\vec{\eta}_k^{\mathrm{T}}S_{22}K_p\vec{r}_{k+1} + 2\vec{\eta}_k^{\mathrm{T}}S_{23}\vec{r}_{k+1} + \vec{r}_{k+1}^{\mathrm{T}}K_p^{\mathrm{T}}S_{22}K_p\vec{r}_{k+1} + 2\vec{r}_{k+1}^{\mathrm{T}}K_p^{\mathrm{T}}S_{23}\vec{r}_{k+1} = \vec{\eta}_k^{\mathrm{T}}S_{22}\vec{\eta}_k + 2\vec{\eta}_k^{\mathrm{T}}(S_{22}K_p + S_{23})\vec{r}_{k+1} + C_{\text{const}} = \vec{\eta}_k^{\mathrm{T}}S_{22}\vec{\eta}_k + C_{\text{const}}$, where $C_{\text{const}} = \vec{r}_{k+1}^{\mathrm{T}}K_p^{\mathrm{T}}S_{23}\vec{r}_{k+1}$. Clearly, $\min_{\vec{c}_k} \tilde{J}_k$ is equivalent to (18). The proof is completed. ■

Under the constraints in (17), the Lyapunov matrix $S$ is designed in Theorem 2.

*Theorem 2:* The matrix $S$ that is used to formulate the Lyapunov function $Z_k^{\mathrm{T}}SZ_k$ and parameterize the upper limit of cost function (18) can be calculated by solving the optimization problem below $\forall i = 1, 2, \ldots, h$

$$\begin{aligned} & \min \ \operatorname{trace}(S) \\ & \text{s.t.} \begin{bmatrix} -S & \diamond & \diamond & \diamond \\ R\Gamma_{ui} & -R & \diamond & \diamond \\ Q\Gamma_{xi} & 0 & -Q & \diamond \\ L\Psi_i & 0 & 0 & S - L - L^{\mathrm{T}} \end{bmatrix} < 0 \end{aligned} \tag{19}$$

where $L$ is a slack variable. When (19) is solved, $S_{22}$, $S_{23}$, and $K_p$ can thus be determined.

*Proof:* Let $V_{Z,k+j} = Z_{k+j}^{\mathrm{T}}SZ_{k+j}$, $j \ge 0$ be a Lyapunov function of (12). Then, applying the relaxation lemma $-LS^{-1}L^{\mathrm{T}} \le S - L - L^{\mathrm{T}}$ and performing congruence transformation with $\operatorname{diag}\{I, R^{-1}, Q^{-1}, L^{-1}\}$, the inequality (19)

guarantees $\begin{bmatrix} -S & \diamond & \diamond & \diamond \\ \Gamma_{ui} & -R^{-1} & \diamond & \diamond \\ \Gamma_{xi} & 0 & -Q^{-1} & \diamond \\ \Psi_i & 0 & 0 & -S^{-1} \end{bmatrix} < 0$. Based on the Schur complement lemma, this inequality further implies that $-S + \Psi_i^{\mathrm{T}} S \Psi_i + \Gamma_{xi}^{\mathrm{T}} Q \Gamma_{xi} + \Gamma_{ui}^{\mathrm{T}} R \Gamma_{ui} < 0 \ \ \forall i = 1, 2, \ldots, h$. Given any nonzero $Z_{k+j}$, we can directly derive $Z_{k+j}^{\mathrm{T}}(-S + \Psi_i^{\mathrm{T}} S \Psi_i + \Gamma_{xi}^{\mathrm{T}} Q \Gamma_{xi} + \Gamma_{ui}^{\mathrm{T}} R \Gamma_{ui}) Z_{k+j} < 0$. By (12) and convex combinations of the vertices of the LPV system, we then can deduce $Z_{k+j+1}^{\mathrm{T}} S Z_{k+j+1} - Z_{k+j}^{\mathrm{T}} S Z_{k+j} + Z_{k+j}^{\mathrm{T}}(\Gamma_x^{\mathrm{T}}(\theta_k) Q \Gamma_x(\theta_k) + \Gamma_u^{\mathrm{T}}(\theta_k) R \Gamma_u(\theta_k)) Z_{k+j} < 0$. Summing up this inequality from $j = 0$ to $j = \infty$, we can obtain $\sum_{j=0}^{\infty} Z_{k+j}^{\mathrm{T}}(\Gamma_x^{\mathrm{T}}(\theta_k) Q \Gamma_x(\theta_k) + \Gamma_u^{\mathrm{T}}(\theta_k) R \Gamma_u(\theta_k)) Z_{k+j} < V_{Z,k}$. Clearly, it implies that (14) can be bounded by $V_{Z,k}$, which further means that the cost function (2) can be bounded by $Z_k^{\mathrm{T}} S Z_k$. Therefore, by using $S$ with minimized trace to parameterize (18), the real-time optimization of the cost function can thus be achieved through minimizing $\vec{\eta}_k^{\mathrm{T}} S_{22} \vec{\eta}_k$. The proof of Theorem 2 is completed. ∎

Based on Theorem 2 and the relation $c_k = K_c \vec{c}_k$, we then can determine the PR gain by $K_r = K_c K_p$. Moreover, the augmented autonomous model (12) can also be redefined as

$$Y_{k+1} = \Omega(\theta_k) Y_k, \ \text{s.t.} \ K_{Yx} Y_k \in \bar{\mathbb{X}}, \ K_{Yu} Y_k \in \bar{\mathbb{U}} \tag{20}$$

where $Y_k = \begin{bmatrix} x_k^{\mathrm{T}} & \vec{\eta}_k^{\mathrm{T}} & \vec{r}_{k+1}^{\mathrm{T}} \end{bmatrix}^{\mathrm{T}}$, $K_{Yx} = \begin{bmatrix} I & 0 & 0 \end{bmatrix}$, $K_{Yu} = \begin{bmatrix} K_e & K_c & K_r + (K_{ur}(\theta_k) - K e K_{xr}(\theta_k)) C_r \end{bmatrix}$, and $\Omega(\theta_k) = \begin{bmatrix} \Phi(\theta_k) & B(\theta_k) K_c & B(\theta_k) K_r + (I - \Phi(\theta_k)) K_{xr}(\theta_k) C_r \\ 0 & A_c & 0 \\ 0 & 0 & A_r \end{bmatrix}$.

Similar to solving $\mathbb{S}_{\mathrm{FTAR}}^{c}$ in (13), the following $\mathbb{S}_{\mathrm{FTAR}}$ of (20) can be further computed:

$$\mathbb{S}_{\mathrm{FTAR}}^{\eta} = \left\{ x : \exists \vec{\eta}_k, \ \text{s.t.} \ \mathcal{M}^{\eta} x_k + \mathcal{N}^{\eta} \vec{\eta}_k + \mathcal{P}^{\eta} \vec{r}_{k+1} \le b^{\eta} \right\}. \tag{21}$$

Finally, the integrated offline design and online implementation steps of the robust PR-based predictive FTTC strategy are summarized in Algorithm 1.

### C. Design of PR- and RG-Based Robust Predictive FTTC

In the previous designs, the variable $\zeta_k$ in RG is assumed to be 0, which means that the predictive regulation beyond $\eta_{k+n_c}$ is not considered or needed. This scenario would hold only if the states have entered into its RPI-set. However, it may be much conservative when some serious faults or fast reference changes are difficult to be tolerant within $n_c$ steps. In this case, RG should be activated to generate an artificial command. This command will be used to compensate the tracking deviations from the desired reference. Note that such handling is beneficial to ensure the feasibility of FTTC optimization. Thus, for the case when Algorithm 1 is not feasible, the additional adjustment by RG can still continue achieving fault tolerance.

Once RG is included, the dynamics of $\vec{\eta}_k$ will change to $\vec{\eta}_{k+1} = A_c \vec{\eta}_k + B_c \zeta_{k+n_c}$ with $B_c = \begin{bmatrix} 0 & I \end{bmatrix}^{\mathrm{T}}$. A straightforward way to integrate RG into FTTC optimization is to modify the reference dynamics in (21). Specifically, we can introduce an offset by turning the desired terminal set point $r_{k+n_r}$ into a new artificial and admissible set point $\hat{r}_{k+n_r} = r_{k+n_r} + F(\theta_{k+n_r}) \zeta_{k+n_r}$, where $F^{+}(\theta_k) = C(I - \Phi(\theta_k))^{-1} B(\theta_k)$.

**Algorithm 1** PR-Based Constrained FTTC

**Off-line Design:** Given system (1), cost function (2) and sets ($\mathbb{X}$, $\mathbb{U}$, $\mathbb{W}$, $\mathbb{F}$). Complete the following designs:

1: Select suitable prediction horizon $n_c$ and previewable horizon $n_r$ according to $n_r \ge n_c \ge n$.
2: Calculate the control gain $K_e$ by solving Theorem 1; Calculate $S$ by solving Theorem 2 and further construct $K_p$ and $K_r$ according to (17) and $K_r = K_c K_p$.
3: Construct $\mathcal{M}^{\eta}$, $\mathcal{N}^{\eta}$, $\mathcal{P}^{\eta}$, $b^{\eta}$ based on Remark 4, (13), and (20).

**On-line Implementation:** Set state $x_0$ and perform the following actions $\forall k \ge 0$:

4: Collect $x_k$, $u_{k-1}^{p\eta}$, $\theta_k$, $r_k$; Calculate $H(\theta_{k-1})$, $K_{xr}(\theta_k)$, $K_{ur}(\theta_k)$; Define $\vec{r}_{k+1}^{\mathrm{T}} \leftarrow \begin{bmatrix} r_{k+1} & \cdots & r_{k+n_r} \end{bmatrix}$.
5: Calculate $x_{r,k} \leftarrow K_{xr}(\theta_k) r_{k+1}$, $u_{r,k} \leftarrow K_{ur}(\theta_k) r_{k+1}$, $\hat{f}_k \leftarrow H(\theta_{k-1})(x_k - A(\theta_{k-1}) x_{k-1} - B(\theta_{k-1}) u_{k-1}^{p\eta})$.
6: Solve

$$\vec{\eta}_k^{*} \leftarrow \min_{\vec{\eta}_k} \ \vec{\eta}_k^{\mathrm{T}} S_{22} \vec{\eta}_k, \ s.t. \ \mathcal{M}^{\eta} x_k + \mathcal{N}^{\eta} \vec{\eta}_k + \mathcal{P}^{\eta} \vec{r}_{k+1} \le b^{\eta}$$

7: Perform

$$u_k^{p\eta} \leftarrow K_e(x_k - x_{r,k}) - \hat{f}_k + u_{r,k} + K_c \vec{\eta}_k^{*} + K_r \vec{r}_{k+1} \tag{22}$$

8: Apply $u_k^{p\eta}$ to control the system.
9: $k \leftarrow k + 1$ and go to step 4.

Clearly, this handling can regulate $\vec{r}_{k+1}$ by adding extra DOF $\zeta_{k+n_r}$. Hence, it is natural to see that the volume of $\mathbb{S}_{\mathrm{FTAR}}$ can thus be enlarged and the feasibility of (22) can also be reinforced. Based on these settings, a PR- and RG-based predictive FTTC can be configured as $u_k^{p\eta\zeta} = K_e(x_k - x_{r,k}) - \hat{f}_k + u_{r,k} + K_c \vec{\eta}_k + K_r(\vec{r}_{k+1} + C_{\mathrm{end}} F(\theta_{k+n_r}) \zeta_{k+n_r})$, where $C_{\mathrm{end}} = \begin{bmatrix} 0 & 0 & \cdots & I \end{bmatrix}^{\mathrm{T}}$.

*Remark 7:* Since $\zeta_{k+n_r}$ can be searched to optimize the propagation effect of $F(\theta_{k+n_r}) \zeta_{k+n_r}$ according to the system status, $F(\theta_{k+n_r})$ in $u_k^{p\eta\zeta}$ is replaced by $F(\theta_k)$ for practicality. In addition, $\vec{\eta}_k$ can be linked to $\zeta_{k+n_r}$ by defining $\vec{\eta}_{k+1} = A_c \vec{\eta}_k + B_c \zeta_{k+n_r}$, where $\eta_k$ beyond $k + n_c$ is restricted to be depended on $\zeta_{k+n_r}$. Generally, there is $n_r \ge n_c$.

In the sequel, by feeding (10) with $u_k^{p\eta\zeta}$ and performing a similar constraint contraction as (12), a new autonomous augmented dynamic model that contains $\zeta_{k+n_r}$ can be obtained

$$X_{k+1} = \Xi(\theta_k) X_k, \ \text{s.t.} \ K_{Xx} X_K \in \bar{\mathbb{X}}, \ K_{Xu} X_k \in \bar{\mathbb{U}} \tag{23}$$

where $\Xi(\theta_k) = \begin{bmatrix} \Phi(\theta_k) & B(\theta_k) K_c & \Xi_{13}(\theta_k) & \Xi_{14}(\theta_k) \\ 0 & A_c & 0 & B_c \\ 0 & 0 & A_r & 0 \\ 0 & 0 & 0 & I \end{bmatrix}$, $\Xi_{13}(\theta_k) = B(\theta_k) K_r + (I - \Phi(\theta_k)) K_{xr}(\theta_k) C_r$, $\Xi_{14}(\theta_k) = B(\theta_k) K_r C_{\mathrm{end}} F(\theta_k)$, $\zeta_{k+n_r+1} = \zeta_{k+n_r}$, $X_k = \begin{bmatrix} x_k^{\mathrm{T}} & \vec{\eta}_k^{\mathrm{T}} & \vec{r}_{k+1}^{\mathrm{T}} & \zeta_{k+n_r}^{\mathrm{T}} \end{bmatrix}^{\mathrm{T}}$, $K_{Xx} = \begin{bmatrix} I & 0 & 0 & 0 \end{bmatrix}$, and $K_{Xu} = \begin{bmatrix} K_e & K_c & K_r + (K_{ur}(\theta_k) - K_e K_{xr}(\theta_k)) C_r & K_r C_{\mathrm{end}} F(\theta_k) \end{bmatrix}$.

The augmentation by $X_k$ enables to reconstruct the cost function in (18). Note that $\min_{\vec{\eta}_k} \vec{\eta}_k^{\mathrm{T}} S_{22} \vec{\eta}_k$ in Lemma 1 is equivalent to $\min_{\vec{\eta}_k} \{\sum_{i=0}^{\infty} \eta_{k+i}^{\mathrm{T}} S_c \eta_{k+i}\}$ due to the previous setting $c_{k+n_c} = 0$ (i.e., $\eta_{k+n_c} = 0$).

**Algorithm 2** PR- and RG-Based Constrained FTTC

**Off-line Design:** Given system (1), cost function (2) and sets ($\mathbb{X}$, $\mathbb{U}$, $\mathbb{W}$, $\mathbb{F}$). Complete the following designs:

1: Select suitable prediction horizon $n_c$ and previewable horizon $n_r$ according to $n_r \geq n_c \geq n$.

2: Calculate the control gain $K_e$ by solving Theorem 1; Calculate $S$ by solving Theorem 2 and further construct $K_p$ and $K_r$ according to (17) and $K_r = K_c K_p$.

3: Construct $\mathcal{M}^{\eta\zeta}$, $\mathcal{N}^{\eta\zeta}$, $\mathcal{P}^{\eta\zeta}$, $Q^{\eta\zeta}$, $b^{\eta\zeta}$ based on Remark 4, (13), (21), and (23).

**On-line Implementation:** Set state $x_0$ and perform the following actions $\forall k \geq 0$:

4: Collect $x_k$, $u_{k-1}^{p\eta\zeta}$, $\theta_k$, $r_k$; Calculate $H(\theta_{k-1})$, $K_{xr}(\theta_k)$, $K_{ur}(\theta_k)$, $F(\theta_k)$; Define $\vec{r}_{k+1}^{\mathrm{T}} \leftarrow \left[r_{k+1} \cdots r_{k+n_r}\right]$.

5: Calculate $x_{r,k} \leftarrow K_{xr}(\theta_k) r_{k+1}$, $u_{r,k} \leftarrow K_{ur}(\theta_k) r_{k+1}$, $\hat{f}_k \leftarrow H(\theta_{k-1})(x_k - A(\theta_{k-1})x_{k-1} - B(\theta_{k-1})u_{k-1}^{p\eta\zeta})$.

6: Solve

$$(\vec{\eta}_k^*, \zeta_{k+n_r}^*) \leftarrow \min_{\vec{\eta}_k, \zeta_{k+n_r}} \vec{\eta}_k^{\mathrm{T}} S_{22} \vec{\eta}_k + T \zeta_{k+n_r}^{\mathrm{T}} S_c \zeta_{k+n_r}$$
$$s.t.\ \mathcal{M}^{\eta\zeta} x_k + \mathcal{N}^{\eta\zeta} \vec{\eta}_k + \mathcal{P}^{\eta\zeta} \vec{r}_{k+1} + Q^{\eta\zeta} \zeta_{k+n_r} \leq b^{\eta\zeta}$$

7: Perform

$$u_k^{p\eta\zeta} \leftarrow K_e(x_k - x_{r,k}) - \hat{f}_k + u_{r,k} + K_c \vec{\eta}_k^* + K_r(\vec{r}_{k+1} + C_{end} F(\theta_k) \zeta_{k+n_r}^*) \quad (26)$$

8: Apply $u_k^{p\eta\zeta}$ to control the system.

9: $k \leftarrow k+1$ and go to step 4.

Here, according to Remark 7, $\eta_{k+n_c}$ is no longer zero since RG is further introduced. Then, we can deduce $\min_{\vec{\eta}_k}\{\sum_{i=0}^{\infty} \eta_{k+i}^{\mathrm{T}} S_c \eta_{k+i}\} = \min_{\vec{\eta}_k}\{\sum_{i=0}^{n_c-1} \eta_{k+i}^{\mathrm{T}} S_c \eta_{k+i} + \sum_{i=n_c}^{\infty} \zeta_{k+n_r}^{\mathrm{T}} S_c \zeta_{k+n_r}\} = \min_{\vec{\eta}_k}\{\vec{\eta}_k^{\mathrm{T}} S_{22} \vec{\eta}_k + \sum_{i=n_c}^{\infty} \zeta_{k+n_r}^{\mathrm{T}} S_c \zeta_{k+n_r}\}$, where $S_c$ is the upper left block of $S_{22}$. It is clear that the above cost function is unbounded whenever $\zeta_{k+n_r} \neq 0$. Hence, a practical method is to introduce the penalty factor for $\sum_{i=n_c}^{\infty} \zeta_{k+n_r}^{\mathrm{T}} S_c \zeta_{k+n_r}$. The following lemma gives an alternative performance index.

*Lemma 2:* The optimization of cost function (2) can be achieved by solving the minimization problem as follows:

$$\min_{\vec{\eta}_k, \zeta_{k+n_r}} \hat{\mathcal{J}} = \vec{\eta}_k^{\mathrm{T}} S_{22} \vec{\eta}_k + T \zeta_{k+n_r}^{\mathrm{T}} S_c \zeta_{k+n_r} \quad (24)$$

where $T$ is a user-specified scalar weighting factor.

Next, $\mathbb{S}_{\mathrm{FTAR}}$ along (23) can be calculated as

$$\mathbb{S}_{\mathrm{FTAR}}^{\eta\zeta} = \left\{x : \exists\left(\vec{\eta}_k, \zeta_{k+n_r}\right) \text{ s.t. } \mathcal{M}^{\eta\zeta} x_k + \mathcal{N}^{\eta\zeta} \vec{\eta}_k + \mathcal{P}^{\eta\zeta} \vec{r}_{k+1} + Q^{\eta\zeta} \zeta_{k+n_r} \leq b^{\eta\zeta}\right\}. \quad (25)$$

By taking $\hat{r}_{k+n_r}$ into (21), (25) can also be quickly obtained.

Based on the reformulated constraint (25) and the cost function index (24), Algorithm 2 can then be summarized to explain the design and implementation steps of the PR- and RG-based constrained FTTC strategy.

To better describe the implementations of Algorithm 2, a block diagram is further provided in Fig. 1.

*Remark 8:* The real-time implementation of the constrained FTTC in Algorithm 2 (or Algorithm 1) needs to rely on the parameters of both offline and online designs. The computational complexity of the offline design mainly comes from the construction of invariant sets $\mathbb{S}_{\mathrm{FTAR}}^{\eta\zeta}$ (or $\mathbb{S}_{\mathrm{FTAR}}^{\eta}$). Fortunately, some iterative algorithms or toolboxes (e.g., [35]–[37]) can be used to solve this problem effectively. Accordingly, the computational complexity of the online design mainly comes from the determinations of $(\vec{\eta}_k^*,\ \zeta_{k+n_\tau}^*)$ since it is necessary to solve a quadratic programming problem. Usually, the typical MATLAB function *quadprog* or efficient algorithm *qpOASES* [38] can be embedded online to determine their optimal values.

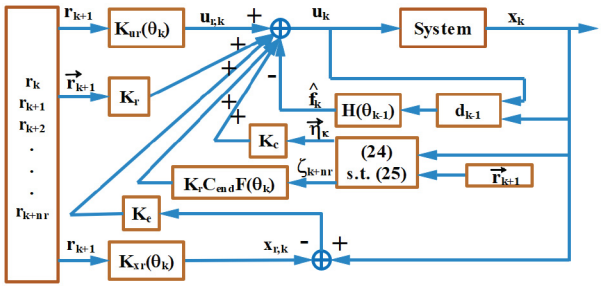


Fig. 1. Block diagram of Algorithm 2.

*Remark 9:* The above constructed algorithms have two main novelties compared with the recently reported predictive FTTC methods (e. g., [18], [21]). First, the constructed PR-based predictive FTTC policy in Algorithm 1 can significantly improve the fault-tolerant tracking transient behavior since the previewable information of reference is systematically integrated to prepare suitable action in advance. This design is beneficial to speed up the tracking response and reduce the overshoot caused by fault compensation error and tracking error. Second, Algorithm 2 further embeds the RG to enlarge the fault-tolerant admissible region such that the fault tolerance feasibility can be robustly guaranteed even in the event of serious fault estimation error and fast change of reference. Actually, these characteristics can also be verified intuitively by the observation that the proposed FTTC policy (26) [or (22)] can include the FTC controllers of [18] and [21] as special cases if we set $K_r = 0$ and $\zeta_{k+n_r} = 0$ in Algorithms 1 and 2.

### *D. Guarantees of Feasibility, Stability, and Optimality*

Based on Theorems 1 and 2, we have the following conclusion.

*Theorem 3:* The constructed PR-based predictive FTTC policy in Algorithm 1 has guarantee of recursive feasibility; the LPV system controlled by Algorithm 1 has guarantee of stability; and the associated cost function (2) has guarantee of minimization.

*Proof:* See the detailed proof in Appendix A in the supplementary material. ■

*Theorem 4:* The constructed PR- and RG-based predictive FTTC policy in Algorithm 2 has guarantee of recursive feasibility; the LPV system controlled by Algorithm 2 has guarantee of stability; and the associated cost function (2) has guarantee of minimization.

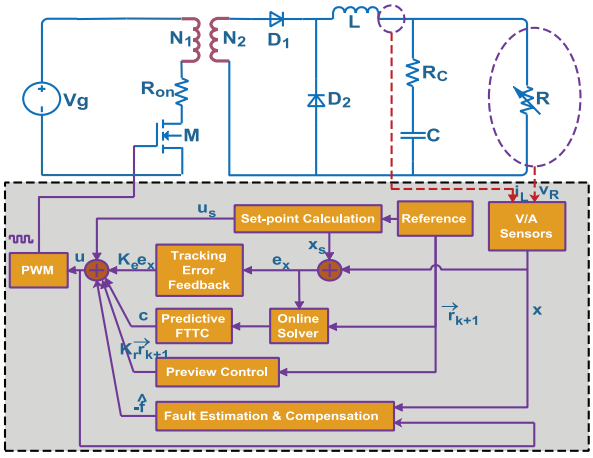


Fig. 2. Electrical control schematic of the dc–dc forward converter.

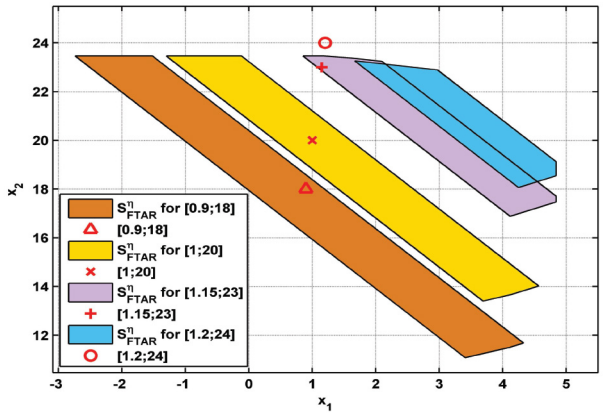


Fig. 3. Comparison of $\mathbb{S}^{\eta}_{\text{FTAR}}$ for different set points obtained by Algorithm 1 (i.e., with embedded PR but without embedded RG).

*Proof:* Following the same lines as proof 4, Theorem 4 can be proved. Due to the page limit, this proof is omitted. ■

## IV. Case Study of DC/DC Forward Converter

### A. LPV Modeling of Forward Converter

A case study of single transistor dc–dc forward converter is given to validate the effectiveness of the proposed optimal predictive FTTC method. The Forward converters, also known as Forward-mode transformers, are used to provide voltage transformation in the manner of circuit isolation. The electrical FTTC schematic of Forward converter is shown in Fig. 2, where the forward-mode controller opens and closes the switch $M$ with the appropriate duty cycle $d$ to adjust the output voltage $v_R$ of Load $R$. The main components and parameters of the converter considered are given in Table I (see Appendix B in the supplementary material), and the modeling steps are explained in Appendix C in the supplementary material.

Further based on the synthesis method in [40], an averaged model describing the whole behaviors of $v_R$ and $i_L$ over a switching period can be obtained

$$\dot{i}_L = -\frac{1}{L}v_R + \frac{V_g N_2}{LN_1}d, \dot{v}_R = \frac{1}{C}i_L - \frac{1}{RC}v_R - \frac{1}{C}i_{\text{Load}}. \quad (27)$$

Next, define $x_t = \begin{bmatrix} i_L & v_R \end{bmatrix}^{\text{T}}$, $u_t = d$, and a sampling time $T_s = 5\times10^{-5}$. Furthermore, considering $V_g \in [V_{g,\min}, V_{g,\max}]$, a discretized two-vertex LPV state-space model of (27) can be obtained as

$$x_{k+1} = \sum_{i=1}^{2} \theta_i(V_{g,k})\{Ax_k + B_i d_k + W\omega_k\} \quad (28)$$

where $A = I + T_s\begin{bmatrix} 0 & -1/L \\ 1/C & -1/RC \end{bmatrix}$, $W = T_s\begin{bmatrix} 0 \\ -1/C \end{bmatrix}$, $B = T_s\begin{bmatrix} \frac{V_{g,k}N_2}{LN_1} \\ 0 \end{bmatrix}$, $\theta_1(V_{g,k}) = [(V_{g,k} - V_{g,\min})/(V_{g,\max} - V_{g,\min})]$, $\theta_2(V_{g,k}) = 1 - \theta_1(V_{g,k})$, $B_1 = B|_{V_{g,k}=V_{g,\min}}$, and $B_2 = B|_{V_{g,k}=V_{g,\max}}$.

### B. Numerical Simulation Results

In the numerical simulation, the load voltage $v_R$ is required to track a given reference voltage $r$. For this purpose, $C$ is defined as $\begin{bmatrix} 0 & I \end{bmatrix}$ such that the performance output satisfies $y = Cx = v_R$. In addition, the weighting matrices are chosen as $Q = 0.4I$ and $R = 1$; the constraints are $|x_k| \le \begin{bmatrix} 8 \\ 26 \end{bmatrix}$, $0 < u_k + f_k \le 0.4$; the preview horizon and predictive horizon are given as $n_r = 5$ and $n_c = 2$, respectively; and the actuator fault is set to be $f_k = -0.001(110 - k)$, $k \in [60,\ 110]$; $f_k = 0.21\sin(20/(2\pi)(k - 150))$, $k \in [150,\ 160]$; $f_k = 0$, else. The reference is $r_k = 18$ V, $k < 150$ and $r_k = 23$ V(or 24 V), $k \ge 150$. The involved optimization problems are solved via MATLAB software. In addition, the numerical simulation duration time is $k = 290$ and the Simulink simulation time $t = 0.02$.

First, the comparisons of $\mathbb{S}_{\text{FTAR}}$ are provided to validate the enhanced fault-tolerant capacity of Algorithm 2 (i.e., the advantages of embedding RG). Based on Algorithm 1, four different $\mathbb{S}^{\eta}_{\text{FTAR}}$ are calculated for set points $\begin{bmatrix} 0.9 & 18 \end{bmatrix}^{\text{T}}$, $\begin{bmatrix} 1 & 20 \end{bmatrix}^{\text{T}}$, $\begin{bmatrix} 1.15 & 23 \end{bmatrix}^{\text{T}}$, and $\begin{bmatrix} 1.2 & 24 \end{bmatrix}^{\text{T}}$, respectively. Their shapes have been depicted in Fig. 3, where it clearly shows that $\mathbb{S}^{\eta}_{\text{FTAR}}$ would change for various set points and their volumes are small. In particular, the set point $\begin{bmatrix} 1.2 & 24 \end{bmatrix}^{\text{T}}$ no longer resides in its $\mathbb{S}^{\eta}_{\text{FTAR}}$. This implies that the set point $\begin{bmatrix} 1.2 & 24 \end{bmatrix}^{\text{T}}$ is an unreachable target for Algorithm 1 and no feasible solution exists in this case. However, as shown in Fig. 4, the systematic inclusion of steady-state offset (i.e., embedded RG in Algorithm 2) allows substantial increases in the volumes of $\mathbb{S}_{\text{FTAR}}$ and the shapes of $\mathbb{S}^{\eta\zeta}_{\text{FTAR}}$ are almost unchanged for the above four set points [see Fig. 4(b)]. Moreover, the subsequent FTTC simulation also shows that the embedded RG in Algorithm 2 can enable a suitable migration of the above unreachable set point $\begin{bmatrix} 1.2 & 24 \end{bmatrix}^{\text{T}}$ of $\mathbb{S}^{\eta}_{\text{FTAR}}$ into an approximated reachable set point of $\mathbb{S}^{\eta\zeta}_{\text{FTAR}}$. This adjustment has been depicted in Fig. 4(a), which shows that Algorithm 2 guarantees the constraint satisfaction for set point $\begin{bmatrix} 1.2 & 24 \end{bmatrix}^{\text{T}}$, albeit in a compromised manner. Based on these discussions, we can verify that RG embedded in Algorithm 2 can enhance the feasibility of constrained FTTC optimization.

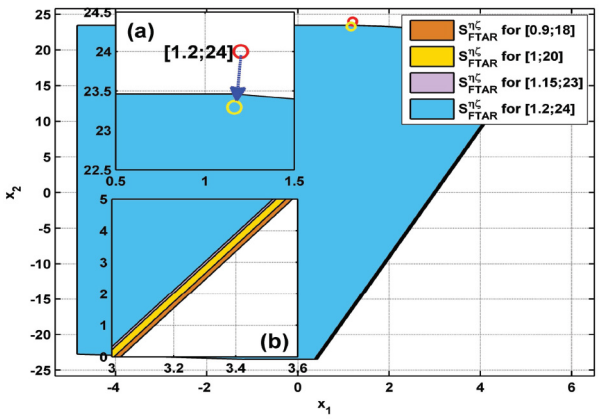


Fig. 4. Comparison of $\mathbb{S}^{\eta\zeta}_{FTAR}$ for different set points obtained by Algorithm 2 (i.e., with embedded PR and embedded RG).

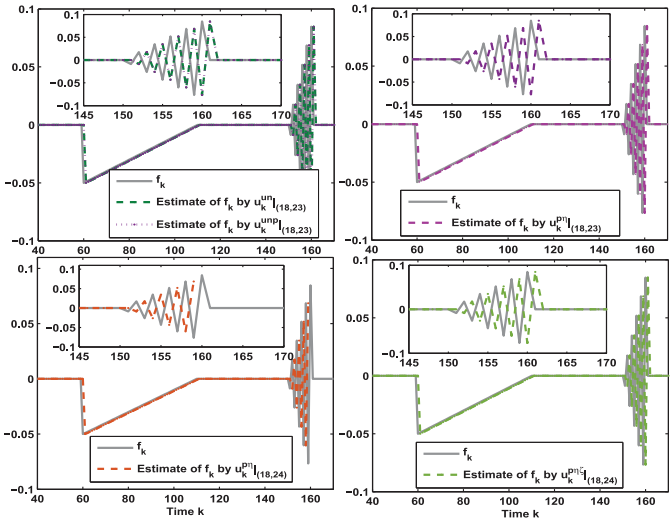


Fig. 5. Comparison of actuator fault estimates for different FTTC policies: $u^{un}$-unconstrained FTTC without PR and RG; $u^{unp}$-unconstrained FTTC with PR but without RG; $u^{p\eta}$-constrained FTTC with PR but without RG (i.e., Algorithm 1); and $u^{p\eta\zeta}$-constrained FTTC with PR and RG (i.e., Algorithm 2). In addition, (18, 23) or (18, 24) represents the piecewise reference satisfying $r_k = 18$ V $\forall k < 150$; $r_k = 23$ V or $r_k = 24$ V $\forall k \geq 150$.

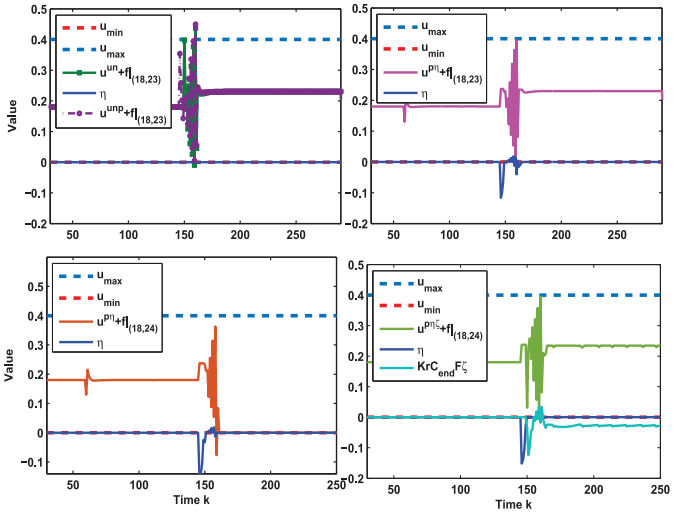


Fig. 6. Comparison of actuator inputs for different FTTC policies.

Second, some numerical simulation results of different FTTC methods are further compared to verify the effectiveness of the proposed algorithms. Without loss of generality, four FTTC strategies are considered, namely, typical robust unconstrained FTTC $u^{un}$, PR-based robust unconstrained FTTC $u^{unp}$, PR-based robust constrained FTTC $u^{p\eta}$ (i.e., Algorithm 1), and PR- and RG-based robust constrained FTTC $u^{p\eta\zeta}$ (i.e., Algorithm 2). The parameters of these control strategies are calculated and listed in Appendix D in the supplementary material. In order to focus on comparisons in terms of transient performance and fault tolerance, the fault estimation and compensation in the above four FTTC strategies are all set to $-H(\theta_{k-1})d_{k-1}$. Based on these settings, the numerical simulation data under the four FTTC strategies are collected in Figs. 5–7. Specifically, Fig. 5 describes the estimation of actuator fault; Fig. 6 gives the FTTC inputs; Fig. 7 shows the load output voltages. Clearly, Fig. 5 illustrates that the intuitive and simple inverse operations by using (5) will generate one-step lag estimation errors. Hence, the corresponding fault compensation will disturb actuator input and change the behavior of the system, especially at the moment when faults appear and disappear. Therefore, the fault-tolerant ability of FTTC methods can be evaluated by checking whether the feasibility can be still guaranteed under such circumstances. In the top-left subfigure of Fig. 6, it can be seen that the faulty actuator inputs under both $u^{un}_k$ and $u^{unp}_k$ exist constraint violations $\forall k \in [150, 160]$. This is mainly caused by the joint influences of fault appearance and reference change. In order to ensure the feasibility, the predictive FTTC policy $u^{p\eta}$ is introduced and the timely effective regulation by $\eta_k$ can be confirmed in the top-right subfigure of Fig. 6. Further by comparing the top-right subfigure and bottom-left subfigure, it can be observed that Algorithm 1 leads to the infeasible problem for target reference $r_k = 24$ V. However, the bottom-right subfigure of Fig. 6 shows that the feasibility to track $r_k = 24$ V can be guaranteed by Algorithm 2 if RG is integrated. These conclusions can be again validated by checking the responses of load voltages in Fig. 7. As expected, the output response with PR is faster than that without PR. In addition, $y^{p\eta}$ by Algorithm 1 becomes infeasible when the reference is set to 24 V [i.e., set point (1.2, 24)]. However, the embedded RG in Algorithm 2 can mitigate an offset such that the output $y^{p\eta\zeta}$ converges to the unreachable set point as close as possible.

### C. Simulation Results Using PLECS Blockset

The effectiveness of the proposed method is further tested in the Simulink environment. Specifically, a dc/dc Forward converter is first built using the PLECS Blockset and the FTTC algorithm is then coded using *S*-function file. Here, a comparative study with [21] is also presented. In theory, due to the integrations of PR and RG, the proposed predictive FTTC method should have faster response time and larger fault-tolerant region. To verify these properties, we still adopt the settings of fault mode and set points in the above numerical simulation. The corresponding simulation results are illustrated in Fig. 8. By comparing the upper (or lower) two curves in

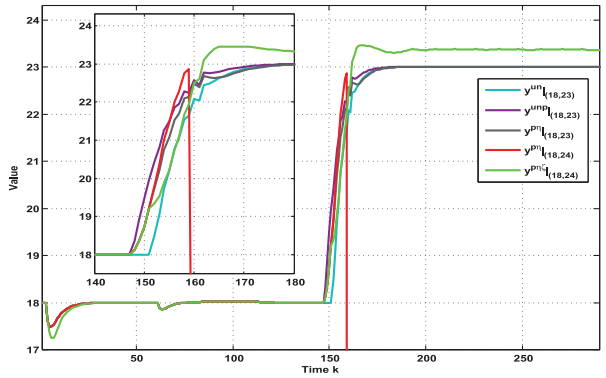


Fig. 7. Comparison of load output voltages for different FTTC policies.

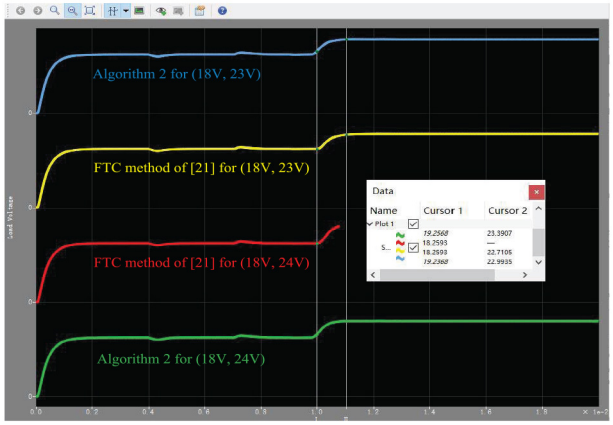


Fig. 8. Comparison of load output voltages in Simulink environment. The curves from top to bottom are generated by Algorithm 2 with reference voltages (18 V, 23 V), the FTC methods in [21] with reference voltages (18 V, 23 V), the FTC methods in [21] with reference voltages (18 V, 24 V), Algorithm 2 with reference voltages (18 V, 24 V), respectively.

Fig. 8, it can be observed that the system transient responses under Algorithm 2 are faster. Moreover, the comparison of cumulative sums of cost function in Table II (see Appendix B in the supplementary material) further illustrates that the application of Algorithm 2 is beneficial to achieve better tracking accuracy. In addition, by comparing the lower two curves in Fig. 8, it can be seen that when the fault appears and the reference changes to 24 V, the predictive FTC method in [21] becomes infeasible whereas Algorithm 2 can still continue to optimizing the tracking. The relevant output voltage and MOSFET PWM input of Algorithm 2 can be checked in Fig. 9. As expected, RG provides an offset such that the final output $v_R$ is regulated to an approximate value around 23.4 V. Although there is no asymptotic tracking of the desired reference 24 V, Algorithm 2 provides an acceptable and feasible solution. On the contrary, the method in [21] is not feasible in this case.

### D. Experimental Results Under Arduino Platform

Finally, the practicability of the proposed algorithm is verified on the Arduino platform. In this test, two Arduino UNO boards are linked to simulate the controller and the Forward converter circuit, respectively. The built experimental prototype is shown in Fig. 10. Specifically, Arduino UNO *A* is

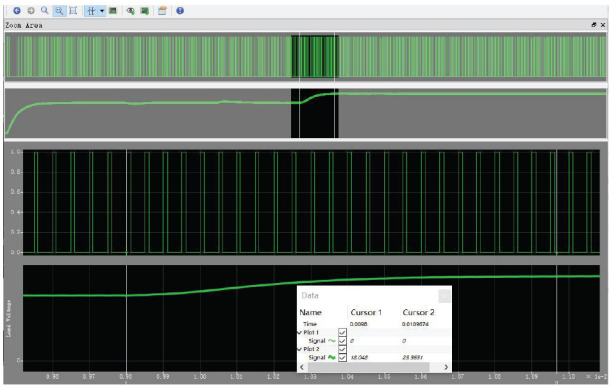

Fig. 9. PWM input and output during fault appears and reference changes.

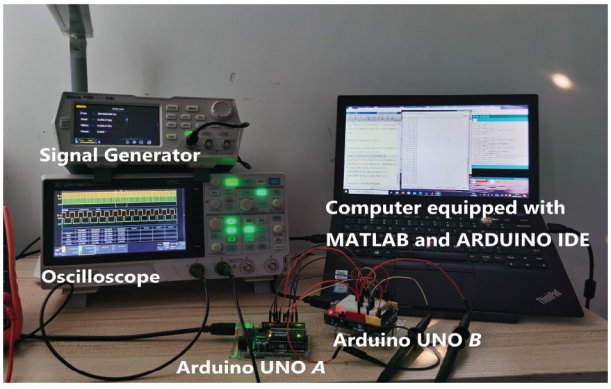


Fig. 10. Experimental setup of converter control.

connected to MATLAB and used as an I/O interface of controller. Arduino UNO *B* receives the signal from the controller and sends the update values of the circuit states. All signals are communicated in the form of PWM. In the customization of the internal program, the reference signal is specified as $r = 18$ V $\forall t \leq 40$ s; $r = 24$ V $\forall t > 40$ s; the fault signal is set as $f = -0.01(30 - t)$ $\forall t \in [20\text{ s},\ 30\text{ s}]$; $f = 0.21\sin(0.3/(t - 40))$ $\forall t \in (40\text{ s},\ 50\text{ s}]$; $f = 0$, else. The test duration is 100 s. Under these same settings, Algorithm 2 in this article and FTC method in [21] have been implemented, respectively. The experimental results of load voltages are collected and shown in Fig. 11. By comparing these two sets of data, the following characteristics can be seen. First, Algorithm 2 has an earlier tracking behavior and faster response when the reference voltage changes from 18 to 24 V. This is not really a surprise, since the PR strategy is integrated into Algorithm 2. Second, similar to the conclusions verified by the aforementioned numerical simulations, Algorithm 2 has stronger fault tolerance. Clearly, the FTC method in [21] is no longer feasible after $t = 54$ s, while Algorithm 2 relies on the offset regulation provided by RG to guarantee the feasibility even if the target is not reachable. Third, the root mean square error (RMSE) has been calculated for both sets of data over the time interval [1 s, 54 s]. Specifically, RMSE of Algorithm 2 is 1.3180, while RMSE of FTC method in [21] is 1.6745. Clearly, Algorithm 2 provides better tracking performance, both in terms of accuracy and fault tolerance. In summary,

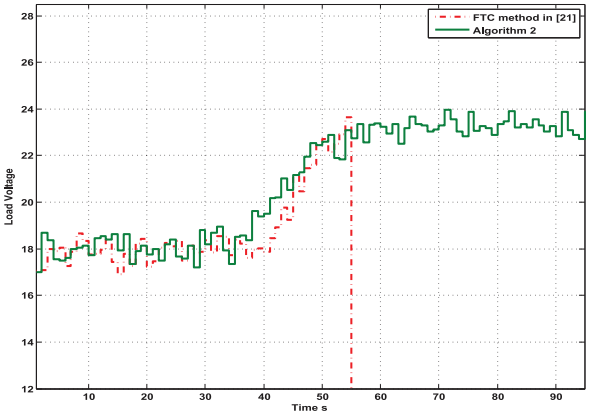


Fig. 11. Comparison of experimental results of the FTC method in [21] and Algorithm 2.

the above discussions have again demonstrated the benefits of integrating PR and RG into predictive FTTC.

## V. Conclusion

The constrained FTTC problem for a class of LPV systems was considered in this article. By introducing PR and RG techniques in dual-mode prediction, a novel predictive FTTC strategy was constructed. Compared with the relevant results in the literature, both closed-loop transient response and fault-tolerant capacity have been improved. The simulation with detailed discussions was also given to demonstrate the benefits of the proposed method. It should be noted that several solutions can be further combined to enhance the obtained results of this article. For instance, the introduction of the Laguerre and Kautz parameterization method can further enlarge the region of attraction; the extension of event-triggered mechanism can speed up the regulation of FTTC optimization. Moreover, the extension to practical converters/inverters or to deal with multiplicative fault deserves further study.

## References

[1] M. Blanke, M. Kinnaert, J. Lunze, and M. Staroswiecki, *Diagnosis and Fault-Tolerant Control*. Berlin, Germany: Springer, 2006.

[2] Z. Gao, C. Cecati, and S. Ding, "A survey of fault diagnosis and fault-tolerant techniques—Part I: Fault diagnosis with model-based and signal-based approaches," *IEEE Trans. Ind. Electron.*, vol. 62, no. 6, pp. 3757–3767, Jun. 2015.

[3] S. Yin, B. Xiao, S. X. Ding, and D. Zhou, "A review on recent development of spacecraft attitude fault tolerant control system," *IEEE Trans. Ind. Electron.*, vol. 63, no. 5, pp. 3311–3320, May 2016.

[4] J.-J. Yan, G.-H. Yang, and X.-J. Li, "Adaptive fault-tolerant compensation control for T–S fuzzy systems with mismatched parameter uncertainties," *IEEE Trans. Syst., Man, Cybern., Syst.*, vol. 50, no. 9, pp. 3412–3423, Sep. 2020.

[5] C. Liu, B. Jiang, R. J. Patton, and K. Zhang, "Integrated fault-tolerant control for close formation flight," *IEEE Trans. Aerosp. Electron. Syst.*, vol. 56, no. 2, pp. 839–852, Apr. 2019.

[6] Z. Zhao, Y. Yang, S. X. Ding, and L. Li, "Fault-tolerant control for systems with model uncertainty and multiplicative faults," *IEEE Trans. Syst., Man, Cybern., Syst.*, vol. 50, no. 2, pp. 514–524, Feb. 2020.

[7] S. Sui, S. Tong, C. L. P. Chen, and K. Sun, "Fuzzy adaptive optimal control for nonlinear switched systems with actuator hysteresis," *Int. J. Adapt. Control Signal Process.*, vol. 33, no. 4, pp. 609–625, Apr. 2019.

[8] Y. Yuan, Z. Wang, L. Guo, and H. Liu, "Barrier Lyapunov functions-based adaptive fault tolerant control for flexible hypersonic flight vehicles with full state constraints," *IEEE Trans. Syst., Man, Cybern., Syst.*, vol. 50, no. 9, pp. 3391–3400, Sep. 2020.

[9] M. Kordestani, M. Saif, M. Orchard, R. Roozbeh, and K. Khashayar, "Failure prognosis and applications—A survey of recent literature," *IEEE Trans. Rel.*, vol. 70, no. 2, pp. 728–748, Jun. 2021.

[10] J. Maciejowski and C. Jones, "MPC fault-tolerant flight control case study: Flight 1862," in *Proc. 5th IFAC SAFEPROCESS*, vol. 36, Jun. 2003, pp. 119–124.

[11] X. Yang and J. M. Maciejowski, "Fault-tolerant model predictive control of a wind turbine benchmark," in *Proc. 8th IFAC SAFEPROCESS*, vol. 45, Jan. 2012, pp. 337–342.

[12] D. Robles, V. Puig, C. Ocampo-Martinez, and L. E. Garza-Castanonet, "Reliable fault-tolerant model predictive control of drinking water transport networks," *Control Eng. Pract.*, vol. 55, pp. 197–211, Oct. 2016.

[13] M. G. Zarch, V. Puig, J. Poshtan, and M. A. Shoorehdeli, "Actuator fault tolerance evaluation approach of nonlinear model predictive control systems using viability theory," *J. Process Control*, vol. 71, pp. 35–45. Nov. 2018.

[14] L. Ferranti, Y. Wan, and T. Keviczky, "Fault-tolerant reference generation for model predictive control with active diagnosis of elevator jamming faults," *Int. J. Robust Nonlinear Control*, vol. 29, no. 16, pp. 5412–5428, Nov. 2019.

[15] R. McCloy, J. De Dona, and M. Seron, "Fault-tolerant fusion-based MPC with sensor recovery for constrained LPV systems," *Int. J. Robust Nonlinear. Control*, vol. 28, no. 11, pp. 3589–3605, Apr. 2018.

[16] R. Sheikhbahaei, A. Alasty, and G. Vossoughi, "Robust fault tolerant explicit model predictive control," *Automatica*, vol. 97, pp. 248–253, Nov. 2018.

[17] E. N. Pistikopoulos, "Perspectives in multiparametric programming and explicit model predictive control," *AIChE J.*, vol. 55, no. 8, pp. 1918–1925, Jun. 2009.

[18] M. Witczak, M. Buciakowski, and C. Aubrun, "Predictive actuator fault-tolerant control under ellipsoidal bounding," *Int. J. Adapt. Control Signal Process.*, vol. 30, no. 2, pp. 375–392, Feb. 2016.

[19] F. A. De Almeida, "Reference management for fault-tolerant model predictive control," *J. Guid. Control Dyn.*, vol. 34, no. 1, pp. 44–56, Jan. 2011.

[20] P. Witczak, M. Pazera, K. Patan, and M. Witczak, "Constrained actuator fault tolerant control with the application to a wind turbine," in *Proc. 10th IFAC SAFEPROCESS*, vol. 51, 2018, pp. 1157–1163.

[21] K. Han and J. Feng, "Reduced-order estimator-based efficient fault-tolerant tracking control optimization for constrained LPV systems," *IEEE Trans. Syst., Man, Cybern., Syst.*, vol. 51, no. 9, pp. 5855–5866, Sep. 2021.

[22] S. S. Dughman and J. A. Rossiter, "Systematic and effective embedding of feedforward of target information into MPC," *Int. J. Control*, vol. 93, no. 1, pp. 98–112, 2020.

[23] M. T. Watson, D. T. Gladwin, T. J. Prescott, and S. O. Conran, "Dual-mode model predictive control of an Omnidirectional wheeled inverted pendulum," *IEEE/ASME Trans. Mechatronics*, vol. 24, no. 6, pp. 2964–2975, Dec. 2019.

[24] R. Nazari, M. M. Seron, and J. A. De Dona, "Actuator fault tolerant control of systems with polytopic uncertainties using set-based diagnosis and virtual-actuator-based reconfiguration," *Automatica*, vol. 75, pp. 182–190, Jan. 2017.

[25] Y. Li, K. Sun, and S. Tong, "Observer-based adaptive fuzzy fault-tolerant optimal control for SISO nonlinear systems," *IEEE Trans. Cybern.*, vol. 49, no. 2, pp. 649–661, Feb. 2049.

[26] Z. Wang, P. Shi, and C. C. Lim, "$H_-/H_\infty$ fault detection observer in finite frequency domain for linear parameter-varying descriptor systems," *Automatica*, vol. 86, pp. 38–45, Dec. 2017.

[27] S. Sui, C. L. P. Chen, and S. Tong, "Fuzzy adaptive finite-time control design for nontriangular stochastic nonlinear systems," *IEEE Trans. Fuzzy Syst.*, vol. 27, no. 1, pp. 172–184, Jan. 2019.

[28] X.-H. Chang, J. Xiong, Z.-M. Li, and J. H. Park, "Quantized static output feedback control for discrete-time systems," *IEEE Trans. Ind. Informat.*, vol. 14, no. 8, pp. 3426–3435, Aug. 2018.

[29] Z. Wang, M. Rodrigues, D. Theilliol, and Y. Shen, "Actuator fault estimation observer design for discrete-time linear parameter-varying descriptor systems," *Int. J. Adapt. Control Signal Process.*, vol. 29, no. 2, pp. 242–258, Jan. 2014.

[30] X. Zhao, P. Shi, and X. Zheng, "Fuzzy adaptive control design and discretization for a class of nonlinear uncertain systems," *IEEE Trans. Cybern.*, vol. 46, no. 6, pp. 1476–1483, Jun. 2016.

[31] S. Sui, C. L. P. Chen, and S. Tong, "Neural network filtering control design for nontriangular structure switched nonlinear systems in finite time," *IEEE Trans. Neur. Net. Learn. Syst.*, vol. 30, no. 7, pp. 2153–2162, Jul. 2019.

[32] W. Xiao, L. Cao, H. Li, and R. Lu, "Observer-based adaptive consensus control for nonlinear multi-agent systems with time-delay," *Sci. China Inf. Sci*, vol. 63, no. 3, pp. 185–201, 2020.
[33] Y. Li, K. Sun, and S. Tong, "Adaptive fuzzy robust fault-tolerant optimal control for nonlinear large-scale systems," *IEEE Trans. Fuzzy Syst.*, vol. 26, no. 5, pp. 2899–2914, Oct. 2018.
[34] K. Han, J. Feng, Y. Li, and S. Li, "Reduced-order simultaneous state and fault estimator based fault tolerant preview control for discrete-time linear time-invariant systems," *IET Control Theory Appl.*, vol. 12, no. 11, pp. 1601–1610, 2018.
[35] F. Blanchini and S. Miani, *Set-Theoretic Methods in Control*. Boston, MA, USA: Birkhauser, 2008.
[36] B. Pluymers, J. A. Rossiter, J. A. K. Suykens, and B. De Moor, "The efficient computation of polyhedral invariant sets for linear systems with polytopic uncertainty," in *Proc. Amer. Control Conf. (ACC)*, 2005, pp. 804–809.
[37] M. Herceg, M. Kvasnica, C. N. Jones, and M. Morari, "Multi-parametric toolbox 3.0," in *Proc. Eur. Control Conf. (ECC)*, 2013, pp. 502–510.
[38] H. Ferreau, C. Kirches, A. Potschka, H. Bock, and M. Diehl, "qpOASES: A parametric active-set algorithm for quadratic programming," *Math. Program. Comput.*, vol. 6, no. 4, pp. 327–363, 2014.
[39] B. Kouvaritakis and M. Cannon, *Model Predictive Control: Classical, Robust and Stochastic*. Cham, Switzerland: Springer, 2016.
[40] B. Choi, *Pulsewidth Modulated DC-to-DC Power Conversion: Circuits, Dynamics, and Control Designs*. Hoboken, NJ, USA: Wiley, 2013.

**Kezhen Han** was born in Zibo, China, in 1988. He received the Ph.D. degree in control theory and control engineering from Northeastern University, Shenyang, China, in 2017.

Since then, he joined the School of Electrical Engineering, University of Jinan, Jinan, Shangdong, China. His main research interests include robust filtering, optimal control, fault diagnosis, fault-tolerant control, and their applications in power electronic circuits.

**Jian Feng** (Member, IEEE) received the B.S., M.S., and Ph.D. degrees in control theory and control engineering from Northeastern University, Shenyang, China, in 1993, 1996, and 2005, respectively.

He is a Professor, a Doctoral Supervisor, and the Vice Head of the Electric Automation Institute, Northeastern University. He has authored and coauthored over 120 journal and conference papers, three monographs, and co-invented 80 patents. His main research interests are fault diagnosis, signal processing, neural networks, and their industrial applications.

Prof. Feng was awarded the New Century Excellent Talents in University in 2008.

**Yueyang Li** (Member, IEEE) received the B.Sc. and Ph.D. degrees in control theory and control engineering from Shandong University, Jinan, China, in 2006 and 2011, respectively.

In 2014, he was a Visiting Scholar with the Center for Robotics, Shandong University. In 2015, he was a Visiting Scholar with the Institute for Automatic Control and Complex Systems, University of Duisburg–Essen, Duisburg, Germany. He is currently the Vice Dean and an Associate Professor with the School of Electrical Engineering, University of Jinan, Jinan. His main research interests include fault diagnosis for time-varying systems, robust filtering for stochastic systems, and their applications to robotics and multidimensional systems.

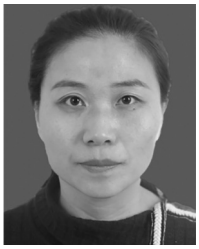

**Ping Jiang** received the Ph.D. degree in detection technology and automation device from Tianjin University, Tianjin, China, in 2010.

She is currently an Associate Professor with the School of Electronic Engineering, University of Jinan, Jinan, China. She had finished her postdoctoral research from 2013 to 2017 with Shandong University, Jinan. Her research interests include image processing, fusion of multi-information, and process control.

**Xiaohong Wang** received the Ph.D. degree in control theory and control engineering from Northeastern University, Shenyang, China, in 2005.

He is currently a Professor with the School of Electronic Engineering, University of Jinan, Jinan, China. He has been committed to the automation, intellectualization, and standardization of process control in process industry for a long time, and has made remarkable achievements in theoretical research and engineering practice of intelligent manufacturing in building materials industry.